PCCP

COMMUNICATION

View Article Online
View Journal | View Issue

Cite this: *Phys. Chem. Chem. Phys.*, 2014, **16**, 7681

Received 22nd December 2013,
Accepted 28th February 2014

DOI: 10.1039/c3cp55395g

www.rsc.org/pccp

Enhanced sensitivity of electron-nuclear double resonance (ENDOR) by cross polarisation and relaxation†

Roberto Rizzato[a] and Marina Bennati*[ab]

Electron-nuclear double resonance (ENDOR) is a method of choice to detect magnetic nuclei in the coordination sphere of paramagnetic molecules, but its sensitivity substantially suffers from saturation effects. Recently we introduced a new pulsed ENDOR experiment based on electron-nuclear cross polarisation (CP) transfer. Here we analyse the time evolution of the spin polarization in CP-ENDOR and show that CP combined with inherent fast relaxation leads to enhanced sensitivity as compared to Davies ENDOR.

Electron-nuclear double resonance (ENDOR) comprises a well-established group of spectroscopic methods that detect magnetic nuclei in the vicinity of paramagnetic centers.[1–4] The technique plays a key role in a wide number of applications ranging from structural investigation of proteins and metalloenzymes[5–8] to catalysis,[9] materials science and quantum information research.[10–13] Specifically, ENDOR is a double frequency experiment in which microwave (mw) and radio frequency (RF) irradiations are used to transfer polarization from electron to nuclear spins. The detection of nuclear spin transitions occurs *via* the electron spins providing much higher sensitivity with respect to a conventional nuclear magnetic resonance (NMR) experiment. Although standard pulse ENDOR, such as Davies and Mims,[1,2] should theoretically deliver a complete transfer of spin polarization (ENDOR effect), in practice this rarely happens due to experimental constraints such as inhomogeneities in the RF field and off-resonance effects in broad lines of powder samples.[14,15] The scarce ENDOR effect needs to be compensated either by a large amount of the sample or by accumulating signals for long times. Therefore, the role of signal averaging combined with spin relaxation becomes of prime importance. Unfortunately, standard pulsed ENDOR techniques require that the waiting time for repetition of the sequence is on the order of the nuclear spin-lattice relaxation time T_{1I}. For experiments performed in frozen solutions at very low temperatures and/or for detecting low-gamma nuclei, this might lead to measurement times of several days. Pulsed ENDOR efficiencies have been analyzed in several papers[3,4,14–18] and modifications of the Davies ENDOR experiment have been proposed, but their performance in powder samples is still not optimal. We have recently proposed[19] a new ENDOR experiment, which utilizes electron-nuclear cross polarization (CP) to polarize ENDOR transitions, as earlier introduced in the context of dynamic nuclear polarization.[20–22] The so-called CP-ENDOR spectra are characterized by an asymmetric intensity of the ENDOR lines, which permits extraction of the relative sign of hyperfine couplings. Moreover, this method appeared insensitive to nuclear saturation effects. In this communication we analyze the time evolution of spin polarization after electron-nuclear cross polarization. We find that the steady state CP-ENDOR polarization is due to the peculiar relaxation behavior related to the asymmetric polarization of the hyperfine lines combined with the effect of the CP sequence.

The CP-ENDOR experiment is illustrated in Fig. 1a. A selective mw 90° pulse excites the magnetization of either the α or the β EPR transition (defined in Fig. 1b). Subsequently, a mw spin-lock pulse with a 90° phase shift is applied for several μs, during which the electron spin system can be considered to be in a *dressed state.*[20,23] Additional RF irradiation induces transitions between pairs of states, if specific resonance conditions (matching conditions) are fulfilled. In a two-spin system $S = 1/2$, $I = 1/2$ there are four possible matching conditions, but in powders only two given by $\Delta\omega_n^{CP} = \pm(\omega_\beta + \omega_\alpha)/2$ lead to a net nuclear polarization effect,[19–21] where ω_α and ω_β are the effective fields of the electron spin in the mw spin-lock frame $\omega_{\alpha/\beta} = \sqrt{(\Delta\omega_e \pm A/2)^2 + \omega_{1e}^2}$, A is the hyperfine (hf) coupling, $\Delta\omega_n^{CP}$ and $\Delta\omega_e$ are the RF-CP and mw field offsets and ω_{1e} is the mw field strength. For sufficiently long irradiation times, the

[a] *Research Group EPR Spectroscopy, Max Planck Institute for Biophysical Chemistry, Am Fassberg 11, 37077 Göttingen, Germany. E-mail: mbennat@gwdg.de; Fax: +49 551 201 1383; Tel: +49 551 201 1911*
[b] *Department of Chemistry, University of Göttingen, Tammanstr. 2, 37077 Göttingen, Germany*

† Electronic supplementary information (ESI) available: Master equations in high temperature approximation; measurement of T_{1I}; global fits of kinetic curves at 94 GHz; and ENDOR intensities as a function of the number of shots. See DOI: 10.1039/c3cp55395g

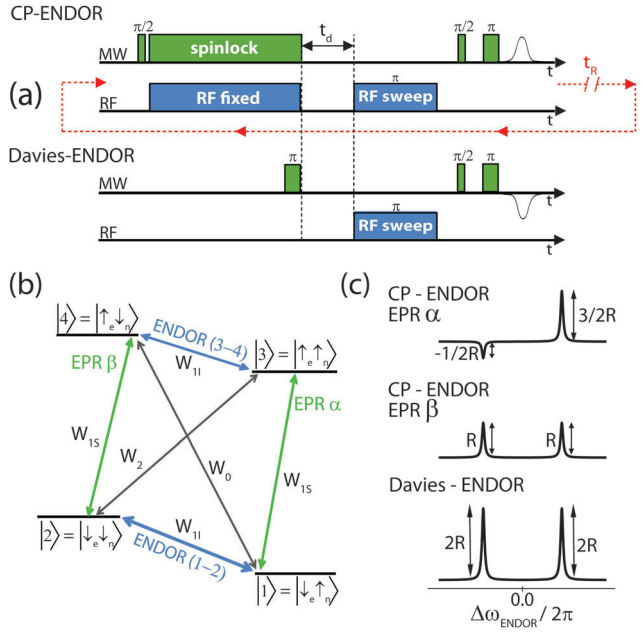

Fig. 1 (a) Time sequence of the CP and Davies ENDOR experiments (see text). (b) The energy scheme for two S = 1/2, I = 1/2 coupled spins showing possible relaxation pathways and rates as well as definitions of EPR and ENDOR transitions. (c) Comparison of ENDOR spectra for one proton I = 1/2 coupled to one electron spin S = 1/2. Line separation corresponds to the hyperfine coupling A. Representative CP-ENDOR intensities for fulfillment of one CP matching condition and selective detection on either the α (top) or β (center) EPR transition. R is a coefficient related to the Boltzmann polarization.

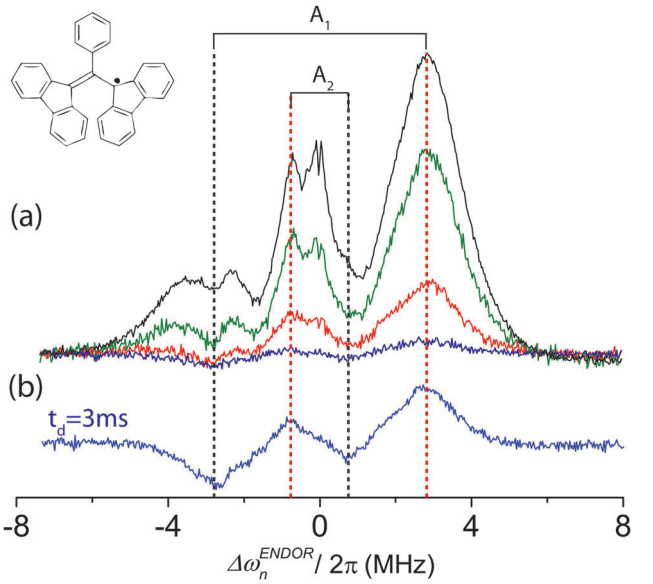

Fig. 2 CP-ENDOR spectra of ^{1}H-BDPA recorded at 34 GHz for increasing t_d. (a) t_d: 2 μs (black); 200 μs (green); 500 μs (red) and 3 ms (blue). (b) The spectrum at 3 ms recorded with longer averaging, *i.e.* 100 scans. Enhanced ENDOR lines are marked with red grids. The line shape dependent inversion of the low-frequency hf line of A_1 is attributed to spectral diffusion. Exp. details: π/2 mw: 100 ns; t_{CP} = 200 μs, π rf = 15 μs, $\Delta\omega_n^{CP}/2\pi = -2.33$ MHz, $\omega_{1e}/2\pi$ = 2.5 MHz; t_r = 20 ms, 512 points; 9 scans; T = 20 K. Random RF acquisition. Acquisition time/spectrum: 1.5 min (a), 17 min (b). Data recorded on a Bruker 580 Elexsys spectrometer with Q-band capabilities (3 W pulse amplifier, Bruker EN 5107D2 Q-Band ENDOR resonator). EPR excitation was in the center of the EPR line. Inset: the structure of BDPA.

effect of the RF is to saturate a matched pair of energy levels and to create a strong non-Boltzmann polarization across the ENDOR lines.[19] Thus, the CP step acts similarly as the preparation π-pulse in Davies ENDOR (Fig. 1a); however, the generated polarization profile is quite different. When a CP condition is met for a spin packet by the appropriate CP-RF offset then the CP-ENDOR intensities depend on the detected electron spin manifold, α or β. The ENDOR lines can have either opposite asymmetric polarization (Fig. 1c, top) or equal and positive polarization (Fig. 1c, center). In the following we denote the first case as an *asymmetric* and the second as a *symmetric* CP-ENDOR spectrum. In a powder sample, detection of EPR α and β transitions from different spin packets occurs concomitantly, resulting in the sum of these two contributions, *i.e.* an absorptive asymmetric CP-ENDOR spectrum. In comparison, the Davies ENDOR spectrum consists of two symmetric lines (Fig. 1c, bottom).

In our previous paper we reported the observation that the CP-ENDOR spectrum is little affected by saturation for repetition times $t_r \leq T_{1S}$, the electron spin-lattice relaxation time, in contrast to the Davies ENDOR. Thus, to be able to investigate kinetics we have varied the time delay t_d between the spin-lock pulse and the rf read out π-pulse (Fig. 1a). The CP-ENDOR spectrum of 0.1% ^{1}H bis-diphenylene-phenyl-allyl (BDPA) in protonated polystyrene matrix at 34 GHz is shown in Fig. 2. At very short t_d the spectrum consists of four lines arising from two hf-couplings of about |1| and |5| MHz. Because the hf couplings have different signs, the enhanced ENDOR lines (Fig. 2, red grids) occur at different sides of the Larmor frequency. By increasing t_d the polarization pattern changes and two ENDOR lines (the non-enhanced ones, Fig. 2 grey grids) become emissive.‡ To analyse the kinetics in more detail, we plotted the intensity of the ENDOR lines at $\Delta\omega_n^{ENDOR}/2\pi = \pm 2.5$ MHz as a function of the time delay t_d. The whole CP-ENDOR spectrum was recorded at each delay time t_d and $S = I_{ENDOR} - I_{ENDOR,baseline}$ was extracted. The obtained decay curves at two different EPR frequencies, *i.e.* 34 and 94 GHz, are displayed in Fig. 3a and b. In all traces the time evolution of nuclear polarization follows a bi-exponential behaviour of the form $S_{ENDOR}(t) = A_1 e^{-t/\tau_1} \mp A_2 e^{-t/\tau_2}$, with a fast and a slow relaxing amplitude. We were able to fit the decay of both ENDOR lines with bi-exponentials of similar values and amplitudes at each respective frequency (Table 1).

The opposite signs for the amplitude coefficients of the slow relaxing component reflect the change in sign of ENDOR lines observed in Fig. 2. To assign the fitted rate values, the electron spin-lattice relaxation time was determined by inversion recovery experiments§ and the nuclear spin-lattice relaxation time T_{1I} of the ENDOR lines at $\Delta\omega_n^{ENDOR} = \pm 2.5$ MHz was estimated by monitoring the signal intensity of Davies ENDOR-spectra as a function of the shot repetition time (SI), as proposed by Tyryshkin *et al.*[14] All values are summarized in Table 1. The data indicate that the measured kinetics reflect an interplay of the electronic T_{1S} and nuclear T_{1I}. We observe that at the considered frequencies and temperature, T_{1I} is one order of magnitude larger than T_{1S}.

To rationalize the effect of spin relaxation during the CP ENDOR experiment, we consider relaxation in the electron-nuclear two-spin system introduced in Fig. 1b. The eigenvectors

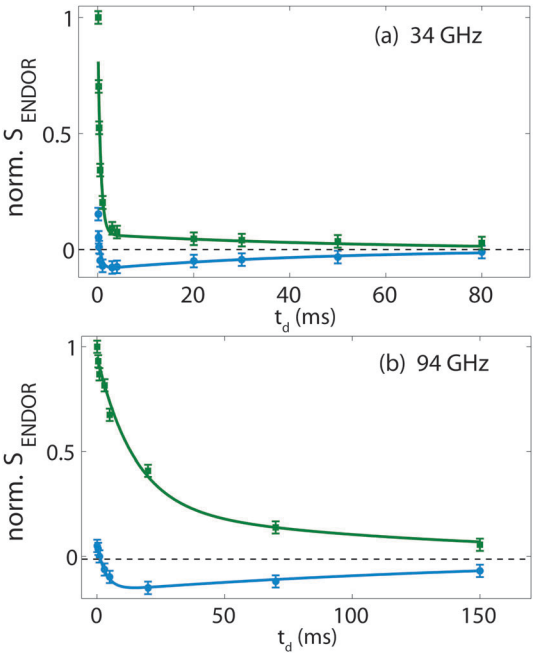

Fig. 3 Intensity of the CP-ENDOR lines at $\Delta\omega_n^{ENDOR}/2\pi$ = +2.5 MHz (green) and −2.5 MHz (blue) as a function of t_d at 34 GHz and T = 20 K (a) and 94 GHz, T = 50 K (b). Exp. conditions for 94 GHz: π/2 mw: 100 ns; t_{CP} = 200 μs, π rf = 28 μs, $\Delta\omega_n^{CP}/2\pi$ = −2.2 MHz, $\omega_{1e}/2\pi$ = 2.5 MHz; t_r = 20–200 ms, 512 points; 16 scans. Random RF acquisition. Temperature values were chosen to satisfy high T approximation. The error bars were estimated from the S/N ratio in the spectra. 34 GHz data were recorded using the set up as shown in Fig. 2. 94 GHz data were recorded using a Bruker E 680 Elexsys spectrometer (Ugrade 2, P = 400 mW) and a cylindrical Bruker EN 680-1021H TeraFlex resonator.

are defined as: $|1\rangle = |\beta_e\alpha_n\rangle$; $|2\rangle = |\beta_e\beta_n\rangle$; $|3\rangle = |\alpha_e\alpha_n\rangle$; $|4\rangle = |\alpha_e\beta_n\rangle$. Since the ENDOR sequence produces a non-Boltzmann distribution of spin populations across the four states, spin relaxation acts during the time evolution of the spin system. For simplicity we neglect relaxation during the pulses and assume that coherences relax very fast after the pulses.[17] All possible spin-lattice relaxation pathways are illustrated in Fig. 1b. In the high temperature approximation, which allows us to discuss analytical solutions for 34 GHz down to ∼20 K and for 94 GHz down to ∼50 K, the transition probabilities between a pair of levels i and j are the same in both directions, *i.e.* $w_{ij} = w_{ji}$. The distribution of spin populations can be calculated by solving the master equation according to Solomon[24] (SI). Assuming the electron Larmor frequency ω_{0S} to be much larger than the nuclear one, ω_{0I}, and neglecting the nuclear spin Boltzmann polarization, the master equations lead to the following time evolution of the ENDOR lines (ESI†):

$$n_{I1-2}(t) = \frac{1}{4}\left(2e^{-tR_I}(n_{0I1-2} + n_{0I3-4}) + 2e^{-tR_\Delta}n_{0\Delta}\right)$$
$$n_{I3-4}(t) = \frac{1}{4}\left(2e^{-tR_I}(n_{0I1-2} + n_{0I3-4}) - 2e^{-tR_\Delta}n_{0\Delta}\right) \quad (1)$$

where $n_{I1-2,3-4}$ is the population difference of the ENDOR lines 1–2 and 3–4 and $n_{0I1-2,3-4}$ are the initial values at the beginning (t = 0) of the time evolution; $n_{0\Delta} = n_{0I1-2} - n_{0I3-4}$ is the initial difference in population of the ENDOR lines. $R_I = 1/T_{1I} = 2w_{1I} + w_2 + w_0$ is the nuclear spin-lattice relaxation rate and $R_\Delta = 1/T_\Delta = 2w_{1S} + 2w_{1I}$. We note that $R_\Delta = 1/T_\Delta$ is on the same order of the electron spin relaxation rate, defined as $R_S = 1/T_{1S} = 2w_{1S} + w_2 + w_0$. In CP-ENDOR the population distribution depends on the selected matching condition and on the detected EPR manifold. By setting a negative CP-RF offset, as in the experiments in Fig. 2 and 3, the CP condition $\Delta\omega_n^{CP} = -(\omega_\beta + \omega_\alpha)/2$ is selected.[19] To derive the coefficients of eqn (1) during the time evolution t_d we utilized the expressions for the diagonal elements of the density matrix at the end of the CP step, *i.e.* at $t_d = 0 \equiv t_{CP}$, as derived in our recent work for this condition:[19]

$$\rho(t_{CP},\alpha) = \begin{bmatrix}\rho_{11}\\ \rho_{22}\\ \rho_{33}\\ \rho_{44}\end{bmatrix} = \frac{1}{2}\begin{bmatrix}-\frac{R}{2}\\ R\\ -\frac{R}{2}\\ 0\end{bmatrix} \quad (2a)$$

$$\rho(t_{CP},\beta) = \begin{bmatrix}\rho_{11}\\ \rho_{22}\\ \rho_{33}\\ \rho_{44}\end{bmatrix} = \frac{1}{2}\begin{bmatrix}\frac{R}{2}\\ 0\\ -\frac{R}{2}\\ 0\end{bmatrix} \quad (2b)$$

where we distinguish between selective detection on either the α or the β EPR transition; R is a coefficient that for an ideal π/2 spin-lock pulse represents electron Boltzmann polarization. Using $\rho_{ii} - \rho_{jj} = n_{ij}$ eqn (2) gives the population differences of the ENDOR transitions at the beginning of the observed free evolution, as required in eqn (1). At the end of the time evolution t_d, the matrix elements of eqn (2) are denoted by $\rho_{ii}(t_d)$. Subsequently, a selective π RF pulse is applied either on the ENDOR 1–2 or 3–4 transition. The effect of this pulse is to interchange the two matrix elements $\rho_{ii}(t_d)$ and $\rho_{jj}(t_d)$ associated

Table 1 Fit parameters for the kinetic curves of Fig. 3 and measured spin-lattice relaxation times of electron spin and ENDOR lines. The error in the long time constants (τ_2 and T_{1I}) was estimated up to 20%, the one in the short time constants (τ_1 and T_{1S}) about 10%. A fit of the 94 GHz data with shared exponentials is provided in the ESI (Fig. S3) for comparison but some discrepancy between τ_1 and T_{1S} values remains

	A_1	τ_1 (ms)	A_2	τ_2 (ms)	T_{1S} (1) (ms)	T_{1S} (2) (ms)	T_{1I} (ms)
ν_{mw} = 34 GHz							
ENDOR line: +2.5 MHz	+0.88 ± 0.26	0.59	+0.065 ± 0.025	50	0.6	5	40
ENDOR line: −2.5 MHz	+0.19 ± 0.06	0.59	−0.084 ± 0.008	45			
ν_{mw} = 94 GHz							
ENDOR line: +2.5 MHz	+0.77 ± 0.025	15	+0.18 ± 0.14	196	3	22	160
ENDOR line: −2.5 MHz	+0.23 ± 0.02	4	−0.17 ± 0.02	172			

with that transition. For detection on the EPRα transition, the ENDOR effect on the EPR echo is defined as:

$$S(\mathrm{ENDOR}_{1-2}, \mathrm{EPR}_\alpha) \sim [\rho_{11}(t_d) - \rho_{33}(t_d)]_{\text{no-RF}} - [\rho_{22}(t_d) - \rho_{33}(t_d)]_{\mathrm{RF}1-2} = \rho_{11}(t_d) - \rho_{22}(t_d)$$
$$S(\mathrm{ENDOR}_{3-4}, \mathrm{EPR}_\alpha) \sim [\rho_{11}(t_d) - \rho_{33}(t_d)]_{\text{no-RF}} - [\rho_{11}(t_d) - \rho_{44}(t_d)]_{\mathrm{RF}3-4} = \rho_{44}(t_d) - \rho_{33}(t_d) \quad (3)$$

For EPR detection of the β transition the ENDOR signal has the same intensity but a reverse sign. Utilizing the matrix elements of eqn (2a) and (3) in eqn (1) we obtain for the ENDOR intensity S during the free evolution t_d:

$$S(\mathrm{ENDOR}_{1-2}, \mathrm{EPR}_\alpha, t_d) \sim [\rho_{11}(t_d) - \rho_{22}(t_d)] = -\frac{R}{2}\cdot e^{-t_d R_I} - \frac{R}{4}\cdot e^{-t_d R_\Delta}$$
$$S(\mathrm{ENDOR}_{3-4}, \mathrm{EPR}_\alpha, t_d) \sim [\rho_{44}(t_d) - \rho_{33}(t_d)] = +\frac{R}{2}\cdot e^{-t_d R_I} - \frac{R}{4}e^{-t_d R_\Delta} \quad (4)$$

with $n_{0I1-2} = 3\cdot n_{0I3-4} = -3/4R$. Thus, the ENDOR polarization decays bi-exponentially during t_d with a component following $R_I = 1/T_{1I}$ and a second component $R_\Delta = 1/T_\Delta$. The coefficients of the first component have same amplitudes but opposite signs. A different expression results for detection on the EPR-β transition. From eqn (1) and (2b) we obtain:

$$S(\mathrm{ENDOR}_{1-2}, \mathrm{EPR}_\beta, t_d) \sim [\rho_{22}(t_d) - \rho_{11}(t_d)] = -n_{0I1-2}e^{-t_d R_\Delta} = -R/2\cdot e^{-t_d R_\Delta}$$
$$S(\mathrm{ENDOR}_{3-4}, \mathrm{EPR}_\beta, t_d) \sim [\rho_{33}(t_d) - \rho_{44}(t_d)] = -R/2\cdot e^{-t_d R_\Delta} \quad (5)$$

where $n_{0I1-2} = R/2$. In this case, the decay of the ENDOR polarization during t_d is mono-exponential following T_Δ for both lines.

Experimentally, in a powder pattern we expect to observe the sum of contributions from eqn (4) and (5). Further, residual ENDOR effects caused by the initial mw π/2 and mw spin-lock sequence with unmatched CP also contribute to the total ENDOR intensity.[19] Therefore, the amplitudes of the components decaying with T_Δ are considerably larger than those decaying with T_{1I}. This is qualitatively consistent with our experimental finding if we compare the fitted amplitudes A_1 and A_2 of the ENDOR lines at 2.5 MHz (Table 1). However, the most important result concerns the amplitudes A_2 for the slow relaxing components. For both frequencies (34 and 94 GHz), the fitted amplitudes A_2 are of the same size and opposite signs within one ENDOR spectrum, as expected from spin packets that fulfill eqn (4). This is in agreement with the appearance of the spectrum in Fig. 2b at long delay times. The results demonstrate that for $1/R_{1I} \gg t_d \gg 1/R_\Delta$ only polarization from the asymmetric CP-ENDOR spectrum is left and the spectrum becomes completely polarized, according to eqn (4).

Finally, expressions similar to eqn (4) and (5) can be derived for the free evolution of the two-spin spin system during the repetition time t_r after the RF π read-out pulse and selective detection by a π/2 mw pulse. We find here again that the decay is bi-exponential, similar to eqn (4), but with a larger amplitude following T_{1I} and a smaller following T_Δ. Nevertheless, to rationalize the combined effect of the CP sequence and relaxation during signal averaging far out of the high temperature approximation (T = 5 K), where actually most of the ENDOR experiments are carried out,¶ we performed numerical simulations of the time evolution of the populations in the four level system for the repetition of several shots. We followed the master equation approach developed in ref. 17, in which the rate equations are solved numerically, combined with the analytical expressions for the evolution of populations during CP given in our previous work.[19] In Fig. 4, we display the intensities of the ENDOR lines as a function of the ratio t_r/T_{1S} for the three cases of ENDOR spectra discussed here (Fig. 1C). During accumulation we find that a steady-state is reached after about 4 shots (Fig. S4, ESI†). The results show that a repetition time on the order of T_{1S} should be sufficient to recover most (up to 80%) of the asymmetric CP-ENDOR spectrum (blue symbols), but it partially saturates the symmetric spectrum (red) to different extents for

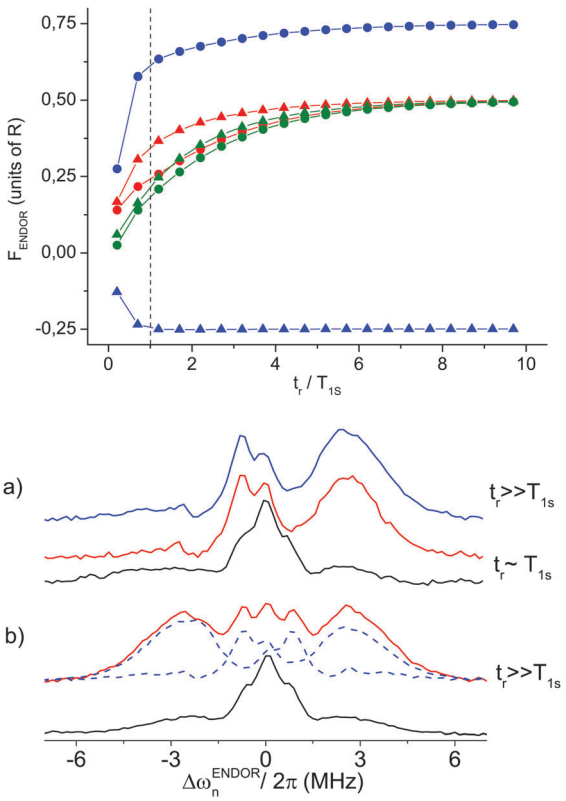

Fig. 4 Top: numerical simulations for the intensities of the ENDOR lines 1–2 (dots) and 3–4 (triangles) in the asymmetric CP-ENDOR (blue), the symmetric CP-ENDOR (red) and residual ENDOR (CP with RF off) after repetition of 4 shots. ν_{EPR} = 94 GHz, T = 5 K, $T_{1I} = T_{1x} = 10\cdot T_{1S}$. T_{1x} is $1/R_x$ or $1/(w_2 - w_0)$. Bottom: the W-band 94 GHz Davies ENDOR spectrum (black) and CP-ENDOR spectra (red/blue) of ^{1}H-BDPA under comparable exp. conditions: (a) black/red: 100 shots/point, t_r = 100 ms, 1 scan. Blue: random RF acquisition, one shot/point, 100 scans. Acquisition time/spectrum: 17 min. (b) Comparison of spectra under random RF acquisition. CP-spectrum (red) is the sum of two spectra (blue dashes) with opposite polarization profile obtained in two consecutive experiments with $\pm\Delta\omega_n^{CP}$. T = 5 K, π/2 mw: 200 ns; t_{CP} = 200 μs, π rf = 25 μs, $\Delta\omega_n^{CP}/2\pi$ = 1.2 MHz. Set up for 94 GHz data as given in caption of Fig. 3.

the two lines. The residual ENDOR effect for non-resonant CP-RF is recovered instead with T_{1I} (green curves).

To examine the situation experimentally, we have recorded CP and Davies ENDOR spectra at low temperatures under comparable experimental conditions. The data are displayed in Fig. 4, bottom. A comparison of spectra for $t_r \approx T_{1S}$ *versus* long repetition times $t_r \gg T_{1S}$ (from random RF acquisition) shows that the intensity of the high frequency line (enhanced in CP-ENDOR spectrum) differs by only 30% whereas in the Davies spectrum by 80%. This is in good qualitative agreement with the predictions from the simulations (we remind that the simulations are performed for an isolated 2-spin system). When comparing the line shapes of the CP-ENDOR spectra at $t_r \approx T_{1S}$ and $t_r \gg T_{1S}$ (red and blue in Fig. 4a) no visible change is observed likely due to a counteracting effect of the relaxing components. In random RF acquisition, saturation of Davies ENDOR is alleviated, but only if T_{1I} is on the order of the acquisition time of one spectrum, as is the case here. The overall signal gain S_{CP}/S_{Davies} in the latter case is 5. Finally, Fig. 4 illustrates that the sum of two CP-ENDOR spectra recorded for a positive and negative CP-RF offset completely recovers the Davies ENDOR line shape, but shows a substantial improvement in S/N.

Conclusions

We have demonstrated that the CP ENDOR experiment can be carried out using a repetition time on the order of the electron spin relaxation time in contrast to standard Davies ENDOR, which requires waiting times on the order of the nuclear spin lattice relaxation. These two relaxation times usually differ by at least one order of magnitude, leading to substantial gain in acquisition time in CP-ENDOR. The observed kinetics are qualitatively consistent with rate equations derived from the previous analytical description of the CP-ENDOR experiments for a two spin-system. Because of the faster acquisition time and the considerable gain in S/N, the CP-ENDOR experiment will potentially provide an attractive alternative to standard Davies ENDOR in several applications. Experiments are in progress to examine the performance of CP-ENDOR with low-gamma nuclei and on real samples.

Acknowledgements

We are indebted to I. Kaminker and S. Vega for critical reading of the manuscript and donation of their Mathematica codes used to cross check our numerical simulations. We would also like to thank N. Enkin and I. Tkach for discussions. The work was supported by the DFG priority program SPP1601 and the Max Planck Society.

Notes and references

‡ A similar effect was reported in ref. 21 but no quantitative analysis was performed.

§ The two values of T_{1S} reflect the bi-exponential inversion recovery curve. The fastest component is attributed to spectral diffusion due to selective excitation in the inhomogeneous EPR line.

¶ Usually, the choice of low temperatures in real samples is dictated by the low intensity of the EPR signals. Particularly in proteins, radical yields are on the order of a few μM, which is at the lowest edge of sensitivity for Davies ENDOR. We note that the BDPA sample, as a model system, does not require low temperatures for ENDOR and the relaxation/saturation issue is alleviated at room temperature. However, we employ here the low temperatures to reproduce the relaxation behaviour and issues of organic radicals in real samples.

1 W. B. Mims, *Proc. R. Soc. London, Ser. A*, 1965, **283**, 452.
2 E. R. Davies, *Phys. Lett. A*, 1974, **47**, 1.
3 C. Gemperle and A. Schweiger, *Chem. Rev.*, 1991, **91**, 1481.
4 A. Grupp and M. Mehring, in *Modern Pulsed and Continuous Wave EPR*, ed. L. Kevan and M. Bowmann, Wiley & Sons, 1990, p. 195.
5 (*a*) T. Argirevic, C. Riplinger, J. Stubbe, F. Neese and M. Bennati, *J. Am. Chem. Soc.*, 2012, **134**, 17661; (*b*) A. J. Fielding, K. Parey, U. Ermler, S. Scheller, B. Jaun and M. Bennati, *J. Biol. Inorg. Chem.*, 2013, **18**, 915.
6 (*a*) N. Cox, D. A. Pantazis, F. Neese and W. Lubitz, *Acc. Chem. Res.*, 2013, **46**(7), 1588; (*b*) A. Silakov, E. J. Reijerse, S. P. J. Albracht, E. C. Hatchikian and W. Lubitz, *J. Am. Chem. Soc.*, 2007, **129**, 11447.
7 B. M. Hoffman, D. Lukoyanov, D. R. Dean and L. C. Seefeldt, *Acc. Chem. Res.*, 2013, **46**(2), 587–595.
8 I. Kaminker, A. Sushenko, A. Potapov, S. Daube, B. Akabayov, I. Sagi and D. Goldfarb, *J. Am. Chem. Soc.*, 2011, **133**, 15514.
9 C. Novara, A. Alfayate, G. Berlier, S. Maurelli and M. Chiesa, *Phys. Chem. Chem. Phys.*, 2013, **15**, 11099.
10 M. M. Mehring, J. Mende and W. Scherer, *Phys. Rev. Lett.*, 2003, **90**, 153001.
11 G. W. Morley, M. Warner, A. M. Stoneham, P. T. Greenland, J. van Tol, C. W. M. Kay and G. Aeppli, *Nat. Mater.*, 2010, **9**, 725.
12 J. J. L. Morton, A. M. Tyryshkin, A. Ardavan, S. C. Benjamin, K. Porfyrakis, S. A. Lyon and G. A. D. Briggs, *Nat. Phys.*, 2006, **2**, 40.
13 S. B. Simmons, R. M. Brown, H. Riemann, N. V. Abrosimov, P. Becker, H. Pohl, M. L. W. Thewalt, K. M. Itoh and J. J. L. Morton, *Nature*, 2011, **470**, 69.
14 A. M. Tyryshkin, J. J. L. Morton, A. Ardavan and S. A. Lyon, *J. Chem. Phys.*, 2006, **124**, 234508.
15 J. J. L. Morton, N. S. Lees, B. M. Hoffman and S. Stoll, *J. Magn. Reson.*, 2008, **191**, 315.
16 M. T. Bennebroek and J. Schmidt, *J. Magn. Reson.*, 1997, **128**, 199.
17 B. Epel, A. Pöppl, P. Manikandan, S. Vega and D. Goldfarb, *J. Magn. Reson.*, 2001, **148**, 388.
18 T. Yang and B. M. Hoffman, *J. Magn. Reson.*, 2006, **181**, 280.
19 R. Rizzato, I. Kaminker, S. Vega and M. Bennati, *Mol. Phys.*, 2013, **111**, 2809.
20 V. Weis, M. Bennati, M. Rosay and R. G. Griffin, *J. Chem. Phys.*, 2000, **113**, 6795.
21 V. Weis and R. G. Griffin, *Solid State Nucl. Magn. Reson.*, 2006, **29**, 105.
22 N. Pomplun, B. Heitmann, N. Khaneja and S. J. Glaser, *Appl. Magn. Reson.*, 2008, **34**, 331.
23 G. Jeschke, *Chem. Phys. Lett.*, 1999, **301**, 524.
24 I. Solomon, *Phys. Rev.*, 1955, **99**, 559.